PHYSICAL REVIEW D 93, 051103(R) (2016)

Measurement of parity-violating spin asymmetries in $W^{\pm}$ production at midrapidity in longitudinally polarized $p+p$ collisions

A. Adare,[13] C. Aidala,[39,44] N. N. Ajitanand,[63] Y. Akiba,[57,58] R. Akimoto,[12] J. Alexander,[63] M. Alfred,[23] K. Aoki,[32,57] N. Apadula,[28,64] Y. Aramaki,[12,57] H. Asano,[35,57] E. C. Aschenauer,[7] E. T. Atomssa,[64] T. C. Awes,[53] B. Azmoun,[7] V. Babintsev,[24] M. Bai,[6] X. Bai,[11] N. S. Bandara,[43] B. Bannier,[64] K. N. Barish,[8] B. Bassalleck,[50] S. Bathe,[5,58] V. Baublis,[56] C. Baumann,[7] S. Baumgart,[57] A. Bazilevsky,[7] M. Beaumier,[8] S. Beckman,[13] R. Belmont,[13,44,68] A. Berdnikov,[60] Y. Berdnikov,[60] D. Black,[8] D. S. Blau,[34] J. S. Bok,[50,51] K. Boyle,[58] M. L. Brooks,[39] J. Bryslawskyj,[5] H. Buesching,[7] V. Bumazhnov,[24] S. Butsyk,[50] S. Campbell,[14,28] C.-H. Chen,[58,64] C. Y. Chi,[14] M. Chiu,[7] I. J. Choi,[25] J. B. Choi,[10] S. Choi,[62] R. K. Choudhury,[4] P. Christiansen,[41] T. Chujo,[67] O. Chvala,[8] V. Cianciolo,[53] Z. Citron,[64,69] B. A. Cole,[14] M. Connors,[64] N. Cronin,[45,64] N. Crossette,[45] M. Csanád,[17] T. Csörgő,[70] S. Dairaku,[35,57] T. W. Danley,[52] A. Datta,[43,50] M. S. Daugherity,[1] G. David,[7] K. DeBlasio,[50] K. Dehmelt,[64] A. Denisov,[24] A. Deshpande,[58,64] E. J. Desmond,[7] O. Dietzsch,[61] L. Ding,[28] A. Dion,[28,64] P. B. Diss,[42] J. H. Do,[71] M. Donadelli,[61] L. D'Orazio,[42] O. Drapier,[36] A. Drees,[64] K. A. Drees,[6] J. M. Durham,[39,64] A. Durum,[24] S. Edwards,[6] Y. V. Efremenko,[53] T. Engelmore,[14] A. Enokizono,[53,57,59] H. En'yo,[57,58] S. Esumi,[67] K. O. Eyser,[7,8] B. Fadem,[45] N. Feege,[64] D. E. Fields,[50] M. Finger,[9] M. Finger, Jr.,[9] F. Fleuret,[36] S. L. Fokin,[34] J. E. Frantz,[52] A. Franz,[7] A. D. Frawley,[19] Y. Fukao,[32,57] T. Fusayasu,[47] K. Gainey,[1] C. Gal,[64] P. Gallus,[15] P. Garg,[3] A. Garishvili,[65] I. Garishvili,[38] H. Ge,[64] F. Giordano,[25] A. Glenn,[38] X. Gong,[63] M. Gonin,[36] Y. Goto,[57,58] R. Granier de Cassagnac,[36] N. Grau,[2] S. V. Greene,[68] M. Grosse Perdekamp,[25] Y. Gu,[63] T. Gunji,[12] H. Guragain,[20] T. Hachiya,[57] J. S. Haggerty,[7] K. I. Hahn,[18] H. Hamagaki,[12] H. F. Hamilton,[1] S. Y. Han,[18] J. Hanks,[64] S. Hasegawa,[29] T. O. S. Haseler,[20] K. Hashimoto,[57,59] R. Hayano,[12] S. Hayashi,[12] X. He,[20] T. K. Hemmick,[64] T. Hester,[8] J. C. Hill,[28] R. S. Hollis,[8] K. Homma,[22] B. Hong,[33] T. Horaguchi,[67] T. Hoshino,[22] N. Hotvedt,[28] J. Huang,[7,39] S. Huang,[68] T. Ichihara,[57,58] H. Iinuma,[32] Y. Ikeda,[57,67] K. Imai,[29] Y. Imazu,[57] J. Imrek,[16] M. Inaba,[67] A. Iordanova,[8] D. Isenhower,[1] A. Isinhue,[45] D. Ivanishchev,[56] B. V. Jacak,[64] M. Javani,[20] S. J. Jeon,[46] M. Jezghani,[20] J. Jia,[7,63] X. Jiang,[39] B. M. Johnson,[7] E. Joo,[33] K. S. Joo,[46] D. Jouan,[54] D. S. Jumper,[25] J. Kamin,[64] S. Kanda,[12,32,57] B. H. Kang,[21] J. H. Kang,[71] J. S. Kang,[21] J. Kapustinsky,[39] K. Karatsu,[35,57] D. Kawall,[43] A. V. Kazantsev,[34] T. Kempel,[28] J. A. Key,[50] V. Khachatryan,[64] P. K. Khandai,[3] A. Khanzadeev,[56] K. Kihara,[67] K. M. Kijima,[22] B. I. Kim,[33] C. Kim,[33] D. H. Kim,[18] D. J. Kim,[30] E.-J. Kim,[10] G. W. Kim,[18] H.-J. Kim,[71] M. Kim,[62] Y.-J. Kim,[25] Y. K. Kim,[21] B. Kimelman,[45] E. Kinney,[13] E. Kistenev,[7] R. Kitamura,[12] J. Klatsky,[19] D. Kleinjan,[8] P. Kline,[64] T. Koblesky,[13] M. Kofarago,[17] B. Komkov,[56] J. Koster,[58] D. Kotchetkov,[52] D. Kotov,[56,60] F. Krizek,[30] K. Kurita,[57,59] M. Kurosawa,[57,58] Y. Kwon,[71] G. S. Kyle,[51] R. Lacey,[63] Y. S. Lai,[14] J. G. Lajoie,[28] A. Lebedev,[28] D. M. Lee,[39] G. H. Lee,[10] J. Lee,[18] K. B. Lee,[39] K. S. Lee,[33] S. Lee,[71] S. H. Lee,[64] S. R. Lee,[10] M. J. Leitch,[39] M. A. L. Leite,[61] M. Leitgab,[25] B. Lewis,[64] X. Li,[11] S. H. Lim,[71] L. A. Linden Levy,[38] M. X. Liu,[39] D. Lynch,[7] C. F. Maguire,[68] Y. I. Makdisi,[6] M. Makek,[69,72] A. Manion,[64] V. I. Manko,[34] E. Mannel,[7,14] T. Maruyama,[29] M. McCumber,[13,39] P. L. McGaughey,[39] D. McGlinchey,[13,19] C. McKinney,[25] A. Meles,[51] M. Mendoza,[8] B. Meredith,[14,25] Y. Miake,[67] T. Mibe,[32] J. Midori,[22] A. C. Mignerey,[42] A. J. Miller,[1] A. Milov,[69] D. K. Mishra,[4] J. T. Mitchell,[7] S. Miyasaka,[57,66] S. Mizuno,[57,67] A. K. Mohanty,[4] S. Mohapatra,[63] P. Montuenga,[25] H. J. Moon,[46] T. Moon,[71] D. P. Morrison,[7,†] M. Moskowitz,[45] T. V. Moukhanova,[34] T. Murakami,[35,57] J. Murata,[57,59] A. Mwai,[63] T. Nagae,[35] S. Nagamiya,[32,57] K. Nagashima,[22] J. L. Nagle,[13,‡] M. I. Nagy,[17,70] I. Nakagawa,[57,58] H. Nakagomi,[57,67] Y. Nakamiya,[22] K. R. Nakamura,[35,57] T. Nakamura,[57] K. Nakano,[57,66] C. Nattrass,[65] P. K. Netrakanti,[4] M. Nihashi,[22,57] T. Niida,[67] S. Nishimura,[12,32] R. Nouicer,[7,58] T. Novák,[31,70] N. Novitzky,[30,64] A. Nukariya,[12] A. S. Nyanin,[34] H. Obayashi,[22] E. O'Brien,[7] C. A. Ogilvie,[28] H. Oide,[12] K. Okada,[58] J. D. Orjuela Koop,[13] J. D. Osborn,[44] A. Oskarsson,[41] H. Ozaki,[67] K. Ozawa,[12,32] R. Pak,[7] V. Pantuev,[26] V. Papavassiliou,[51] I. H. Park,[18] J. S. Park,[62] S. Park,[62] S. K. Park,[33] S. F. Pate,[51] L. Patel,[20] M. Patel,[28] H. Pei,[28] J.-C. Peng,[25] D. V. Perepelitsa,[7,14] G. D. N. Perera,[51] D. Yu. Peressounko,[34] J. Perry,[28] R. Petti,[7,64] C. Pinkenburg,[7] R. Pinson,[1] R. P. Pisani,[7] M. L. Purschke,[7] H. Qu,[1] J. Rak,[30] B. J. Ramson,[44] I. Ravinovich,[69] K. F. Read,[53,65] D. Reynolds,[63] V. Riabov,[49,56] Y. Riabov,[56,60] E. Richardson,[42] T. Rinn,[28] N. Riveli,[52] D. Roach,[68] G. Roche,[40,*] S. D. Rolnick,[8] M. Rosati,[28] Z. Rowan,[5] J. G. Rubin,[44] M. S. Ryu,[21] B. Sahlmueller,[64] N. Saito,[32] T. Sakaguchi,[7] H. Sako,[29] V. Samsonov,[49,56] M. Sarsour,[20] S. Sato,[29] S. Sawada,[32] B. Schaefer,[68] B. K. Schmoll,[65] K. Sedgwick,[8] J. Seele,[58] R. Seidl,[57,58] Y. Sekiguchi,[12] A. Sen,[20,65] R. Seto,[8] P. Sett,[4] A. Sexton,[42] D. Sharma,[64,69] A. Shaver,[28] I. Shein,[24] T.-A. Shibata,[57,66] K. Shigaki,[22] M. Shimomura,[28,48,67] K. Shoji,[57] P. Shukla,[4] A. Sickles,[7,25] C. L. Silva,[39] D. Silvermyr,[41,53] K. S. Sim,[33] B. K. Singh,[3] C. P. Singh,[3] V. Singh,[3] M. Skolnik,[45] M. Slunečka,[9] M. Snowball,[39] S. Solano,[45] R. A. Soltz,[38] W. E. Sondheim,[39] S. P. Sorensen,[65] I. V. Sourikova,[7] P. W. Stankus,[53] P. Steinberg,[7] E. Stenlund,[41] M. Stepanov,[43] A. Ster,[70] S. P. Stoll,[7] M. R. Stone,[13] T. Sugitate,[22] A. Sukhanov,[7] T. Sumita,[57] J. Sun,[64] J. Sziklai,[70] E. M. Takagui,[61] A. Takahara,[12] A. Taketani,[57,58] Y. Tanaka,[47] S. Taneja,[64] K. Tanida,[58,62] M. J. Tannenbaum,[7] S. Tarafdar,[3,69] A. Taranenko,[49,63] E. Tennant,[51] R. Tieulent,[20] A. Timilsina,[28] T. Todoroki,[57,67] M. Tomášek,[15,27] H. Torii,[12,22] C. L. Towell,[1] M. Towell,[1] R. Towell,[1] R. S. Towell,[1] I. Tserruya,[69] Y. Tsuchimoto,[12] C. Vale,[7] H. W. van Hecke,[39] M. Vargyas,[17,70] E. Vazquez-Zambrano,[14] A. Veicht,[14] J. Velkovska,[68] R. Vértesi,[70]

M. Virius,[15] B. Voas,[28] V. Vrba,[15,27] E. Vznuzdaev,[56] X. R. Wang,[51,58] D. Watanabe,[22] K. Watanabe,[57,59] Y. Watanabe,[57,58] Y. S. Watanabe,[12,32] F. Wei,[51] S. Whitaker,[28] A. S. White,[44] S. N. White,[7] D. Winter,[14] S. Wolin,[25] C. L. Woody,[7] M. Wysocki,[13,53] B. Xia,[52] L. Xue,[20] S. Yalcin,[64] Y. L. Yamaguchi,[12,64] A. Yanovich,[24] J. Ying,[20] S. Yokkaichi,[57,58] J. H. Yoo,[33] I. Yoon,[62] Z. You,[39] I. Younus,[37,50] H. Yu,[55] I. E. Yushmanov,[34] W. A. Zajc,[14] A. Zelenski,[6] S. Zhou,[11] and L. Zou[8]

(PHENIX Collaboration)

[1]*Abilene Christian University, Abilene, Texas 79699, USA*
[2]*Department of Physics, Augustana University, Sioux Falls, South Dakota 57197, USA*
[3]*Department of Physics, Banaras Hindu University, Varanasi 221005, India*
[4]*Bhabha Atomic Research Centre, Bombay 400 085, India*
[5]*Baruch College, City University of New York, New York, New York, 10010, USA*
[6]*Collider-Accelerator Department, Brookhaven National Laboratory, Upton, New York 11973-5000, USA*
[7]*Physics Department, Brookhaven National Laboratory, Upton, New York 11973-5000, USA*
[8]*University of California-Riverside, Riverside, California 92521, USA*
[9]*Charles University, Ovocný trh 5, Praha 1, 116 36 Prague, Czech Republic*
[10]*Chonbuk National University, Jeonju 561-756, Korea*
[11]*Science and Technology on Nuclear Data Laboratory, China Institute of Atomic Energy, Beijing 102413, People's Republic of China*
[12]*Center for Nuclear Study, Graduate School of Science, University of Tokyo, 7-3-1 Hongo, Bunkyo, Tokyo 113-0033, Japan*
[13]*University of Colorado, Boulder, Colorado 80309, USA*
[14]*Columbia University, New York, New York 10027 and Nevis Laboratories, Irvington, New York 10533, USA*
[15]*Czech Technical University, Zikova 4, 166 36 Prague 6, Czech Republic*
[16]*Debrecen University, H-4010 Debrecen, Egyetem tér 1, Hungary*
[17]*ELTE, Eötvös Loránd University, H-1117 Budapest, Pázmány P. s. 1/A, Hungary*
[18]*Ewha Womans University, Seoul 120-750, Korea*
[19]*Florida State University, Tallahassee, Florida 32306, USA*
[20]*Georgia State University, Atlanta, Georgia 30303, USA*
[21]*Hanyang University, Seoul 133-792, Korea*
[22]*Hiroshima University, Kagamiyama, Higashi-Hiroshima 739-8526, Japan*
[23]*Department of Physics and Astronomy, Howard University, Washington, DC 20059, USA*
[24]*IHEP Protvino, State Research Center of Russian Federation, Institute for High Energy Physics, Protvino 142281, Russia*
[25]*University of Illinois at Urbana-Champaign, Urbana, Illinois 61801, USA*
[26]*Institute for Nuclear Research of the Russian Academy of Sciences, prospekt 60-letiya Oktyabrya 7a, Moscow 117312, Russia*
[27]*Institute of Physics, Academy of Sciences of the Czech Republic, Na Slovance 2, 182 21 Prague 8, Czech Republic*
[28]*Iowa State University, Ames, Iowa 50011, USA*
[29]*Advanced Science Research Center, Japan Atomic Energy Agency, 2-4 Shirakata Shirane, Tokai-mura, Naka-gun, Ibaraki-ken 319-1195, Japan*
[30]*Helsinki Institute of Physics and University of Jyväskylä, P.O. Box 35, FI-40014 Jyväskylä, Finland*
[31]*Károly Róbert University College, H-3200 Gyöngyös, Mátrai út 36, Hungary*
[32]*KEK, High Energy Accelerator Research Organization, Tsukuba, Ibaraki 305-0801, Japan*
[33]*Korea University, Seoul 136-701, Korea*
[34]*National Research Center "Kurchatov Institute," Moscow, 123098 Russia*
[35]*Kyoto University, Kyoto 606-8502, Japan*
[36]*Laboratoire Leprince-Ringuet, Ecole Polytechnique, CNRS-IN2P3, Route de Saclay, F-91128 Palaiseau, France*
[37]*Physics Department, Lahore University of Management Sciences, Lahore 54792, Pakistan*
[38]*Lawrence Livermore National Laboratory, Livermore, California 94550, USA*
[39]*Los Alamos National Laboratory, Los Alamos, New Mexico 87545, USA*
[40]*LPC, Université Blaise Pascal, CNRS-IN2P3, Clermont-Fd, 63177 Aubiere Cedex, France*
[41]*Department of Physics, Lund University, Box 118, SE-221 00 Lund, Sweden*
[42]*University of Maryland, College Park, Maryland 20742, USA*
[43]*Department of Physics, University of Massachusetts, Amherst, Massachusetts 01003-9337, USA*
[44]*Department of Physics, University of Michigan, Ann Arbor, Michigan 48109-1040, USA*

[45]Muhlenberg College, Allentown, Pennsylvania 18104-5586, USA
[46]Myongji University, Yongin, Kyonggido 449-728, Korea
[47]Nagasaki Institute of Applied Science, Nagasaki-shi, Nagasaki 851-0193, Japan
[48]Nara Women's University, Kita-uoya Nishi-machi Nara 630-8506, Japan
[49]National Research Nuclear University, MEPhI, Moscow Engineering Physics Institute, Moscow 115409, Russia
[50]University of New Mexico, Albuquerque, New Mexico 87131, USA
[51]New Mexico State University, Las Cruces, New Mexico 88003, USA
[52]Department of Physics and Astronomy, Ohio University, Athens, Ohio 45701, USA
[53]Oak Ridge National Laboratory, Oak Ridge, Tennessee 37831, USA
[54]IPN-Orsay, Univ. Paris-Sud, CNRS/IN2P3, Université Paris-Saclay, BP1, F-91406 Orsay, France
[55]Peking University, Beijing 100871, People's Republic of China
[56]PNPI, Petersburg Nuclear Physics Institute, Gatchina, Leningrad Region 188300, Russia
[57]RIKEN Nishina Center for Accelerator-Based Science, Wako, Saitama 351-0198, Japan
[58]RIKEN BNL Research Center, Brookhaven National Laboratory, Upton, New York 11973-5000, USA
[59]Physics Department, Rikkyo University, 3-34-1 Nishi-Ikebukuro, Toshima, Tokyo 171-8501, Japan
[60]Saint Petersburg State Polytechnic University, St. Petersburg 195251, Russia
[61]Universidade de São Paulo, Instituto de Física, Caixa Postal 66318, São Paulo CEP05315-970, Brazil
[62]Department of Physics and Astronomy, Seoul National University, Seoul 151-742, Korea
[63]Chemistry Department, Stony Brook University, SUNY, Stony Brook, New York 11794-3400, USA
[64]Department of Physics and Astronomy, Stony Brook University, SUNY, Stony Brook, New York 11794-3800, USA
[65]University of Tennessee, Knoxville, Tennessee 37996, USA
[66]Department of Physics, Tokyo Institute of Technology, Oh-okayama, Meguro, Tokyo 152-8551, Japan
[67]Center for Integrated Research in Fundamental Science and Engineering, University of Tsukuba, Tsukuba, Ibaraki 305, Japan
[68]Vanderbilt University, Nashville, Tennessee 37235, USA
[69]Weizmann Institute, Rehovot 76100, Israel
[70]Institute for Particle and Nuclear Physics, Wigner Research Centre for Physics, Hungarian Academy of Sciences (Wigner RCP, RMKI) H-1525 Budapest 114, P.O. Box 49, Budapest, Hungary
[71]Yonsei University, IPAP, Seoul 120-749, Korea
[72]University of Zagreb, Faculty of Science, Department of Physics, Bijenička 32, HR-10002 Zagreb, Croatia

(Received 29 April 2015; published 23 March 2016)

We present midrapidity measurements from the PHENIX experiment of large parity-violating single-spin asymmetries of high transverse momentum electrons and positrons from $W^{\pm}/Z$ decays, produced in longitudinally polarized $p + p$ collisions at center of mass energies of $\sqrt{s} = 500$ and 510 GeV. These asymmetries allow direct access to the antiquark polarized parton distribution functions due to the parity-violating nature of the W-boson coupling to quarks and antiquarks. The results presented are based on data collected in 2011, 2012, and 2013 with an integrated luminosity of 240 pb^{-1}, which exceeds previous PHENIX published results by a factor of more than 27. These high Q^2 data probe the parton structure of the proton at W mass scale and provide an important addition to our understanding of the antiquark parton helicity distribution functions at an intermediate Bjorken x value of roughly $M_{\mathrm{W}}/\sqrt{s} = 0.16$.

DOI: 10.1103/PhysRevD.93.051103

The determination of the contributions of partons to the spin of the proton has inspired significant theoretical and experimental effort for several decades [1–13]. The quark contribution to the nucleon spin has been deduced through measurements in polarized inclusive deep-inelastic scattering (DIS) and semi-inclusive deep-inelastic scattering (SIDIS) experiments [6,12–15]. Although the overall quark contribution ($\Delta\Sigma = \Delta q + \Delta\bar{q}$) has been well determined through DIS experiments (in the range $10^{-3} < x < 1$), the contributions from sea quarks separated by flavor (determined through SIDIS experiments) are comparatively poorly known. Data from HERMES and COMPASS [6,16] provide constraints on the contribution from the sea quarks, however, uncertainties in fragmentation functions and the low energy scales of fixed target experiments limit the accuracy with which these measurements can quantitatively determine the sea quark contribution [17]. As

*Deceased.
†morrison@bnl.gov
‡jamie.nagle@colorado.edu

such, an independent measurement using a different technique [18] to determine the contribution from different flavors of sea quarks is desirable.

The use of W-boson production provides just such a solution. Parity is maximally violated in the W couplings to quarks and leptons, so $\mathrm{W}^{\pm}$ production in $p+p$ collisions proceeds only by coupling to left-handed quarks and right-handed antiquarks ($u_L\bar{d}_R \to \mathrm{W}^+$ and $d_L\bar{u}_R \to \mathrm{W}^-$). By measuring decay leptons in the final state, the flavor and helicity state of the colliding quarks can be determined [18–21]. Asymmetries measured in $\mathrm{W}^{\pm}$ by reversing the helicity of a colliding proton are sensitive to the individual quark/antiquark helicity parton distribution functions (PDFs) (Δu, Δd, $\Delta\bar{u}$ and $\Delta\bar{d}$). Moreover, the energy scale for these events, of the order of the W-boson mass, allows for small and precisely calculable higher-order corrections.

We present results for the parity-violating single-spin asymmetry A_L for $p+p \to \mathrm{W}^{\pm}/\mathrm{Z} + X \to e^{\pm} + X'$ at mid-rapidity from 2011–2013 PHENIX data at the Relativistic Heavy Ion Collider (RHIC). These results relate to an intermediate Bjorken x value of roughly $M_{\mathrm{W}}/\sqrt{s} = 0.16$. Initial measurements at RHIC in 2009 accumulated 8.6 pb^{-1} by PHENIX [9] and 12 pb^{-1} by STAR [10,11]. Here, the total integrated luminosity is 240 pb^{-1} at $\sqrt{s} = 500$ GeV in 2011, and at 510 GeV in 2012 and 2013 [22]. Proton-beam polarizations were also considerably improved from ~0.39 in 2009 to 0.50–0.56 in 2011–2013.

The measurements are performed with the two PHENIX central arm spectrometers. Each arm covers $|\Delta\phi| = \pi/2$ in azimuth and $|\eta| < 0.35$ in pseudorapidity. A comprehensive description of the PHENIX detector at RHIC can be found in [23]. The major detector subsystems used for this analysis are the electromagnetic calorimeter (EMCal) and the drift chamber/pad chamber tracking system. Two beam-beam counters located at ± 144 cm from the collision point along the beam line and covering $3.1 < |\eta| < 3.9$ were used to define the minimum bias trigger and to measure the relative luminosity between different colliding bunch pairs.

The data were collected with an EMCal-based trigger [24] with nominal energy threshold of 5.6 GeV, which was fully efficient for $e^{\pm}$ with transverse momentum $p_T^e > 10$ GeV/c. The p_T^e was determined from the energy deposited in the EMCal with energy resolution $\sigma_E/E = 8.1\%/\sqrt{E(\mathrm{GeV})} \oplus 4\%$. The energy resolution was determined from the p_T dependence of the widths of reconstructed π^0 and η meson mass peaks. The same π^0 and η meson mass peaks were used in the energy calibration of the EMCal, and were continuously monitored. Similar to our previous analysis [9] and test beam data results [24], the EMCal energy scale was confirmed to within 2.5%, for the energy range analyzed with this data. A loose time-of-flight cut was applied in the analysis to remove noncollision background.

The tracking system was used for collision vertex reconstruction, track charge sign determination, and background suppression. The main tracking detector, the drift chamber (DC), spanning the radial distance 2.02–2.46 m from the beam line, measured the charged track bending in the axial magnetic field of the PHENIX central magnet, with a field integral of 1.15 Tm. The z coordinate for the tracks was obtained from the pad chambers situated behind the DC. Reconstructed tracks were matched with high energy clusters in the EMCal within a cone angle of 0.02, retaining $> 99\%$ of real $e^{\pm}$ tracks, as determined from simulations. The coordinate information from both the calorimeter and the tracking system was used to determine the z vertex of the event, and only events with $|z| < 30$ cm were used in the analysis.

The charge sign of a track was determined from the bending angle α_{DC}, which is inversely proportional to the track transverse momentum [$\alpha_{\mathrm{DC}}(\mathrm{mrad}) = 92/p_T$ GeV/c]. A region corresponding to $|\alpha_{\mathrm{DC}}| < 1$ mrad was removed in order to minimize the possibility of charge misidentification. This led to $< 3\%$ loss of $e^{\pm}$ from W-boson decays. To further eliminate the charge sign ambiguity in the DC track reconstruction, the regions in the vicinity of anode wires were removed from the analysis, reducing the DC acceptance by ~15%. The remaining opposite charge contribution to the W^- (W^+) signal was 2% (0.4%), as determined using the DC resolution of 1.4 mrad and α_{DC} convoluted over the W decay $e^{\pm}$ p_T distribution. The result is consistent with a full detector simulation.

Accurate momentum reconstruction in the tracking system requires the precise determination of the beam position in the plane orthogonal to the beam line. This was measured and monitored using straight tracks from special runs with the magnetic field off throughout the data taking period.

An isolation cut was very efficient at suppressing background events with a high degree of activity around a candidate electron (as would happen for jet events). The cut parameter r_{iso} was defined as $r_{\mathrm{iso}} = (\Sigma E_i)/E_e$, where E_i is the ith EMCal cluster energy and track p_T around the electron candidate in a cone with a radius in η and ϕ of 0.4, and E_e is the energy of electron candidate. A candidate was kept for the analysis if $r_{\mathrm{iso}} < 0.1$.

Figure 1 shows the resulting yield of electron and positron candidates for the 2013 data set. A Jacobian peak around $p_T^e = 40$ GeV/c corresponds to $e^{\pm}$ from W^- and Z boson decays. The isolation cut removed about 90% of the background (as was evaluated from the background-dominated region between 10 and 20 GeV/c) and left more than 90% of the signal in the Jacobian peak region untouched (as evaluated from simulations explained below). Similar results were obtained for the 2011 and 2012 data sets. Above 30 GeV/c the remaining candidate events after the isolation cut are dominated by W and Z decay to electrons/positrons, and by background events below 25 GeV/c. This background consists mainly of high momentum electrons/positrons from conversion of π^0/η

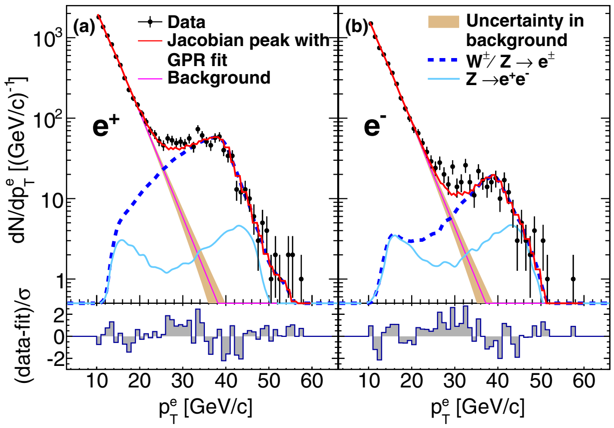

FIG. 1. (Upper panels) Spectra for (a) e^+ and (b) e^- using the EMCal for momentum determination from $p + p$ collisions at $\sqrt{s} = 510$ GeV from 2013. From top to bottom, the curves are the following: solid [red] is the sum between background and signal; shaded band [orange] is the background estimation with the uncertainty from the GPR method; dashed [dark blue] is the $W^\pm/Z \to e^\pm$ signal obtained from simulation normalized to the data; and solid [light blue] is the contribution from $Z \to e^+e^-$. (Lower panels) Point-by-point comparison of the data and the fit result: (data$_i$-fit)/σ_i, where σ_i is statistical uncertainty of the ith data point.

decay photons, charged pions/kaons, $b,c \to e$ decays and accidental matching between high energy EMCal clusters and tracks in the DC. The Z boson contribution in the signal region above 30 GeV/c was estimated to be 7% (25%) for the positrons (electrons) after all analysis cuts were applied, as determined from simulations. The asymmetry of the Z has been estimated theoretically using the DSSV08 PDF sets and measured by the STAR Collaboration [11] to be -0.07 ± 0.14.

Experimentally, the longitudinal single-spin asymmetry is defined as

$$A_L = \frac{1}{P}\frac{N^+ - RN^-}{N^+ + RN^-}, \tag{1}$$

where P is the beam polarization, N^+ (N^-) is the number of events in the signal region for the positive (negative) beam helicity and R is the luminosity ratio (relative luminosity) between positive and negative helicity bunches measured using the minimum bias trigger defined by a coincidence of the two beam-beam counters. The relative luminosity between different helicity combinations did not differ from unity by more than 2%. The asymmetry calculation was performed for events in the p_T range from 30 to 50 GeV/c, which defined the signal region in this analysis. This range was selected to optimize the signal to background. Less than 1% of the signal is expected above 50 GeV/c. Asymmetries obtained in this fashion must be corrected for background events, which are parity conserving, in the signal region. This dilution factor can be defined as $(A - B)/A$, where A (B) is the number of all (background) events in the signal region $30 < p_T < 50$ GeV/c. The final asymmetry values can be obtained by dividing the result by the dilution factor.

The background in the signal region was estimated using the Gaussian process regression (GPR) technique [25–28] to extrapolate the background shape from the background-dominated region to the signal-dominated region. The major advantage of this method is that it does not require an *a priori* known functional form to test against data. At its core, this method allows for the determination of the shape of a set of data points with statistical uncertainties using only the data themselves. Furthermore, the predictions made using this method have a mathematically well-defined Gaussian uncertainty.

Through our use of the radial basis function (RBF) kernel [25,26], we assume a smooth (infinitely differentiable) shape for the background. The background shape was constrained from data points in the p_T ranges 10–22 GeV/c and 60–65 GeV/c, where the signal contribution is expected to be negligible. Although bins in the range 60–65 GeV/c don't contain any events, they still improve the precision of the background evaluation. These empty bins were assigned a statistical uncertainty of 1 count. The background in the signal region is assumed to vary on p_T scales equal or larger than those in the background-dominated regions.

The RBF kernel contains a characteristic length parameter that is an indicator of how far away from data the background extrapolations can be made. For obtained characteristic lengths larger than 30 GeV/c, we concluded that our background estimation (based on data between 10 to 22 GeV/c and 60 to 65 GeV/c) in the signal region (30 to 50 GeV/c) has an appropriate statistical uncertainty.

Table I summarizes the background contributions with statistical uncertainties obtained using the GPR approach along with the counts in the signal region for each data set. The GPR analysis was performed for different p_T ranges for the background estimation and including/excluding the constraint between 60 and 65 GeV/c. The results were within the statistical uncertainty of the full GPR analysis so no additional systematic was added.

In Fig. 1, the background and signal shapes were used to describe the data points. The only fit parameter was the normalization for the signal shape. The signal shape was obtained from a PYTHIA simulation [29] of $W^\pm$ and Z boson decays to electrons/positrons, followed by a full GEANT3-based [30] detector response simulation. The simulated events were analyzed using the analysis package used for the data. The fit quality of the data-driven background shape plus the simulated signal shape is reasonable for both e^- and e^+ spectra.

As a cross check of the background determination, a fit to the data using a phenomenologically motivated modified power law function as the background shape was also

TABLE I. Number of events recorded for e^+ and e^- for $30 < p_T < 50$ GeV/c and the background contributions, dilution factors, and two-beam polarizations for each analyzed data set.

					Polarization	
Lepton	Year	Counts	Background contribution	Dilution factor	B	Y
e^+	2011	70	$2.3 \pm 2.3(\text{stat}) \pm 0.6(\text{syst})$	$0.97 \pm 0.03(\text{stat}) \pm 0.01(\text{syst})$	0.51 ± 0.02	0.50 ± 0.02
	2012	105	$2.5 \pm 2.5(\text{stat})^{+4.7}_{-2.5}(\text{syst})$	$0.98 \pm 0.02(\text{stat})^{+0.02}_{-0.04}(\text{syst})$	0.55 ± 0.02	0.57 ± 0.02
	2013	669	$18.6 \pm 7.3(\text{stat}) \pm 14.9(\text{syst})$	$0.97 \pm 0.01(\text{stat}) \pm 0.02(\text{syst})$	0.55 ± 0.02	0.55 ± 0.02
e^-	2011	27	$1.7 \pm 1.6(\text{stat}) \pm 0.7(\text{syst})$	$0.94 \pm 0.06(\text{stat}) \pm 0.02(\text{syst})$	0.51 ± 0.02	0.50 ± 0.02
	2012	47	$5.5 \pm 4.7(\text{stat}) \pm 2.2(\text{syst})$	$0.88 \pm 0.10(\text{stat}) \pm 0.05(\text{syst})$	0.55 ± 0.02	0.57 ± 0.02
	2013	233	$13.9 \pm 5.6(\text{stat})^{+20.0}_{-13.9}(\text{syst})$	$0.94 \pm 0.02(\text{stat})^{+0.06}_{-0.09}(\text{syst})$	0.55 ± 0.02	0.55 ± 0.02

performed $(f(p_T) = 1/p_T^{\alpha+\beta \ln p_T})$. The discrepancy between the central value results from two methods was assigned as a systematic uncertainty for the background determination. Another source of uncertainty may come from the possible systematic discrepancy between the data points and the fit result in some p_T regions (e.g. data excess over the fit in the vicinity of $p_T = 30$ GeV/c in Fig. 1). Following a conservative approach for uncertainty evaluation, the sum of the signed differences between data points and the fit results within the signal region was assigned as an additional systematic uncertainty. The final systematic uncertainty was obtained by adding in quadrature the systematic uncertainty from the two sources discussed above. Using the GPR-estimated background contamination in the signal region, the dilution factor for each data set was calculated and is presented in Table I.

The asymmetry calculation was done following two independent methods. First the asymmetry was calculated separately for each polarized beam using Eq. (1), with the polarization for the other beam averaged to zero. The final result is a weighted average of asymmetries from two beams. A likelihood method was also used in order to deal with the lower statistics, particularly in the 2011 and 2012 data sets.

The two rings at RHIC with counterpropagating beams are designated yellow (y,Y) and blue (b,B). The number of expected counts μ_{yb} for the data sample can be expressed as

$$\mu_{yb} = R_{yb}N(1 + b \cdot A_L P_B + y \cdot A_L P_Y + b \cdot y \cdot A_{LL} P_B P_Y) \tag{2}$$

where R_{yb} is the relative luminosity between the colliding beam helicity configurations, y (b) denotes the helicity of the two colliding beams and takes the value of $+1$ (-1) for positive (negative) helicity, the parameter N is an average count, P_B and P_Y are the polarizations of the two beams, A_{LL} is the double spin asymmetry. The spin asymmetries were calculated by maximizing a likelihood function defined using Poisson statistics as

$$\mathcal{L} = \prod_{y=\pm1,b=\pm1} \mathcal{P}(\mu_{yb}, N_{yb}), \tag{3}$$

where N_{yb} is the spin sorted yield. To calculate the 2013 positive and negative η bin asymmetries a generalized form for these equations was used.

Table II summarizes the A_L results. Both of the asymmetry calculation methods employed gave consistent results for all the data sets. The systematic uncertainties were obtained by propagating the systematic uncertainties of the dilution factors to the final asymmetry values. A scale uncertainty of 3.5% from the RHIC beam polarization measurements is not included in Table I. The asymmetry in the background region was also measured and for all cases the asymmetry was consistent with zero, within uncertainties.

These results are shown in Fig. 2 with two theoretical calculations: collisions at high energies (CHE) [21] for the NNPDFpol1.1 [14] and a recent calculation [31] using the DSSV 14 PDF sets [32]. While the DSSV 14 curve was obtained from a global fit of DIS and SIDIS data (including recent COMPASS results [15,16]), the NNPDFpol1.1 uncertainty band contains the 2012 STAR [11] result for flavor separation in addition to DIS data. The theoretical asymmetry calculations agree with the data within 1.5σ uncertainty of the data points. These results will be used to further constrain the quark and antiquark polarized parton distributions functions at an intermediate Bjorken x value of roughly $M_{\mathrm{W}}/\sqrt{s} = 0.16$.

Figure 3 shows the combined asymmetry for all of the PHENIX data sets and published data from STAR [11]. The

TABLE II. Longitudinal single-spin asymmetries, A_L, for the 2011 and 2012 data sets (combined) spanning the entire η range of PHENIX ($|\eta| < 0.35$), for the 2013 data set separated into two η bins, and for the combined 2011-2013 data sets.

Lepton	Data set	$\langle\eta\rangle$	A_L
e^+	2011 + 2012	0	$-0.27 \pm 0.10(\text{stat}) \pm 0.01(\text{syst})$
	2013 $\eta > 0$	0.17	$-0.38 \pm 0.07(\text{stat}) \pm 0.01(\text{syst})$
	2013 $\eta < 0$	−0.17	$-0.35 \pm 0.07(\text{stat}) \pm 0.01(\text{syst})$
	2011–2013 all	0	$-0.35 \pm 0.04(\text{stat}) \pm 0.01(\text{syst})$
e^-	2011 + 2012	0	$0.28 \pm 0.16(\text{stat}) \pm 0.02(\text{syst})$
	2013 $\eta > 0$	0.17	$0.10 \pm 0.13(\text{stat})^{+0.02}_{-0.01}(\text{syst})$
	2013 $\eta < 0$	−0.17	$0.17 \pm 0.12(\text{stat})^{+0.03}_{-0.01}(\text{syst})$
	2011–2013 all	0	$0.17 \pm 0.08(\text{stat}) \pm 0.02(\text{syst})$

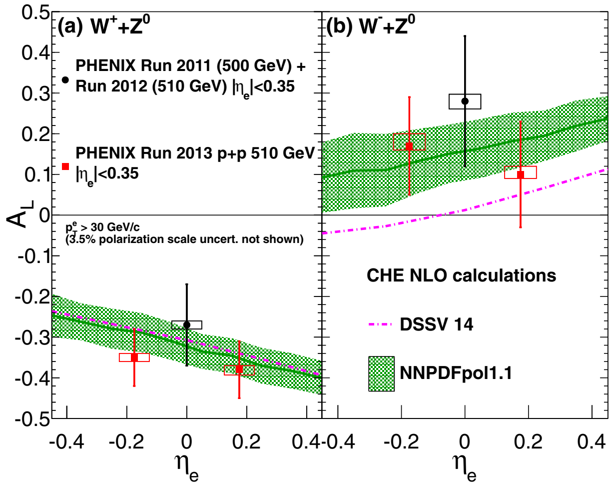

FIG. 2. Asymmetry results from the combined 2011 and 2012 data sets for $|\eta| < 0.35$ (black circles) and the 2013 data (red squares) separated into two equal η bins between -0.35 and 0.35. The green line and shaded region shows a theoretical calculation using CHE [21] with the NNPDFpol1.1 PDF sets [14], while the dashed magenta line shows the DSSV14 calculation [31].

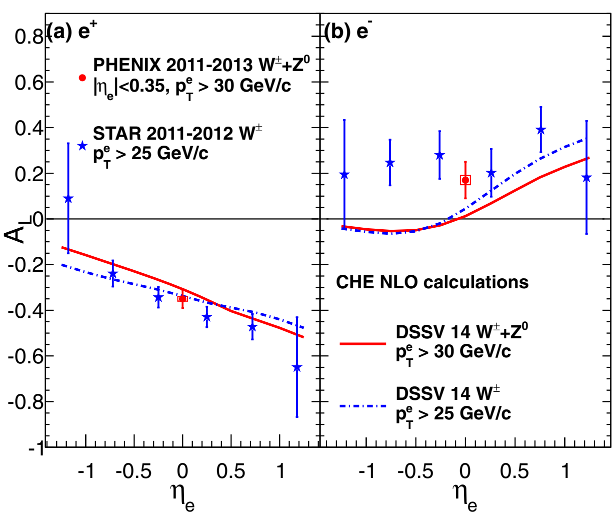

FIG. 3. Asymmetry results from the combined 2011–2013 data sets from PHENIX [red] circles and the STAR 2011–2012 [11] W results [blue] stars and their respective DSSV 14 theoretical predictions.

two data sets cannot be compared directly, because PHENIX measures the asymmetry from $W^\pm + Z$ decays, while the STAR result is solely from $W^\pm$ decays. The comparison can be made through the curves, which account for the specifics of each measurement. Qualitatively, both data sets show the same trend with data points below (above) the central value of the theoretical prediction for W^+ (W^-), for $|\eta| < 0.5$. The W^- difference a larger $\Delta\bar{u}$ contribution in the covered $x \sim 0.16$ range, when compared with the central value of the DSSV 14 PDF fit calculation.

In summary, for high p_T e^- and e^+ from $W^\pm$ and Z boson decays, PHENIX measured the single-spin asymmetries with more than 27 times higher statistics and better polarization compared to 2009 [9]. These new results and the STAR data [11] will help constrain the antiquark PDFs in a global analysis. Asymmetries calculated from global fits based on previous measurements, such as DSSV14 and NNPDFpol1.1, are consistent with our data. The use of the electroweak interaction provides an independent tool to extract quark and antiquark helicity contribution. The data presented here are complementary to previous SIDIS measurements and bring the field one step closer to elucidation of the proton-spin puzzle [1].

We thank the staff of the Collider-Accelerator and Physics Departments at Brookhaven National Laboratory and the staff of the other PHENIX participating institutions for their vital contributions. We acknowledge support from the Office of Nuclear Physics in the Office of Science of the Department of Energy, the National Science Foundation, Abilene Christian University Research Council, Research Foundation of SUNY, and Dean of the College of Arts and Sciences, Vanderbilt University (U.S.), Ministry of Education, Culture, Sports, Science, and Technology and the Japan Society for the Promotion of Science (Japan), Conselho Nacional de Desenvolvimento Científico e Tecnológico and Fundação de Amparo à Pesquisa do Estado de São Paulo (Brazil), Natural Science Foundation of China (People's Republic of China), Croatian Science Foundation and Ministry of Science, Education, and Sports (Croatia), Ministry of Education, Youth and Sports (Czech Republic), Centre National de la Recherche Scientifique, Commissariat à l'Énergie Atomique, and Institut National de Physique Nucléaire et de Physique des Particules (France), Bundesministerium für Bildung und Forschung, Deutscher Akademischer Austausch Dienst, and Alexander von Humboldt Stiftung (Germany), National Science Fund, OTKA, Károly Róbert University College, and the Ch. Simonyi Fund (Hungary), Department of Atomic Energy and Department of Science and Technology (India), Israel Science Foundation (Israel), Basic Science Research Program through NRF of the Ministry of Education (Korea), Physics Department, Lahore University of Management Sciences (Pakistan), Ministry of Education and Science, Russian Academy of Sciences, Federal Agency of Atomic Energy (Russia), VR and Wallenberg Foundation (Sweden), the U.S. Civilian Research and Development Foundation for the Independent States of the Former Soviet Union, the Hungarian American Enterprise Scholarship Fund, and the US-Israel Binational Science Foundation.

[1] J. Ashman *et al.* (European Muon Collaboration), A measurement of the spin asymmetry and determination of the structure function $g(1)$ in deep inelastic muon-proton scattering, Phys. Lett. B **206**, 364 (1988).

[2] R. L. Jaffe and A. Manohar, The $G(1)$ problem: Fact and fantasy on the spin of the proton, Nucl. Phys. **B337**, 509 (1990).

[3] B. Adeva *et al.* (Spin Muon Collaboration), Spin asymmetries $A(1)$ and structure functions $g1$ of the proton and the deuteron from polarized high-energy muon scattering, Phys. Rev. D **58**, 112001 (1998).

[4] P. L. Anthony *et al.* (E155 Collaboration), Measurement of the deuteron spin structure function $g_1^d(x)$ for $1\ (\mathrm{GeV}/c)^2 < Q^2 < 40\ (\mathrm{GeV}/c)^2$, Phys. Lett. B **463**, 339 (1999).

[5] M. Alekseev *et al.* (COMPASS Collaboration), The polarised valence quark distribution from semi-inclusive DIS, Phys. Lett. B **660**, 458 (2008).

[6] A. Airapetian *et al.* (HERMES Collaboration), Quark helicity distributions in the nucleon for up, down, and strange quarks from semi-inclusive deep-inelastic scattering, Phys. Rev. D **71**, 012003 (2005).

[7] A. Adare *et al.* (PHENIX Collaboration), Inclusive double-helicity asymmetries in neutral-pion and eta-meson production in $\vec{p}+\vec{p}$ collisions at $\sqrt{s}=200$ GeV, Phys. Rev. D **90**, 012007 (2014).

[8] L. Adamczyk *et al.* (STAR Collaboration), Precision Measurement of the Longitudinal Double-Spin Asymmetry for Inclusive Jet Production in Polarized Proton Collisions at $\sqrt{s}=200$ GeV, Phys. Rev. Lett. **115**, 092002 (2015).

[9] A. Adare *et al.* (PHENIX Collaboration), Cross Section and Parity Violating Spin Asymmetries of $W^{\pm}$ Boson Production in Polarized $p+p$ Collisions at $\sqrt{s}=500$ GeV, Phys. Rev. Lett. **106**, 062001 (2011).

[10] M. M. Aggarwal *et al.* (STAR Collaboration), Measurement of the Parity-Violating Longitudinal Single-Spin Asymmetry for $W^{\pm}$ Boson Production in Polarized Proton-Proton Collisions at $\sqrt{s}=500$ GeV, Phys. Rev. Lett. **106**, 062002 (2011).

[11] L. Adamczyk *et al.* (STAR Collaboration), Measurement of Longitudinal Spin Asymmetries for Weak Boson Production in Polarized Proton-Proton Collisions at RHIC, Phys. Rev. Lett. **113**, 072301 (2014).

[12] D. de Florian, R. Sassot, M. Stratmann, and W. Vogelsang, Extraction of spin-dependent parton densities and their uncertainties, Phys. Rev. D **80**, 034030 (2009).

[13] E. Leader, A. V. Sidorov, and D. B. Stamenov, Determination of polarized PDFs from a QCD analysis of inclusive and semi-inclusive deep inelastic scattering data, Phys. Rev. D **82**, 114018 (2010).

[14] E. R. Nocera, R. D. Ball, S. Forte, G. Ridolfi, and J. Rojo (The NNPDF Collaboration), A first unbiased global determination of polarized PDFs and their uncertainties, Nucl. Phys. **B887**, 276 (2014).

[15] M. G. Alekseev *et al.* (COMPASS Collaboration), The spin-dependent structure function of the proton g_1^p and a test of the Bjorken sum rule, Phys. Lett. B **690**, 466 (2010).

[16] M. G. Alekseev *et al.* (COMPASS Collaboration), Quark helicity distributions from longitudinal spin asymmetries in muon-proton and muon-deuteron scattering, Phys. Lett. B **693**, 227 (2010).

[17] E. Leader, A. V. Sidorov, and D. B. Stamenov, Impact of CLAS and COMPASS data on polarized parton densities and higher twist, Phys. Rev. D **75**, 074027 (2007).

[18] C. Bourrely and J. Soffer, Parton distributions and parity violating asymmetries in $W^{\pm}$ and Z production at RHIC, Phys. Lett. B **314**, 132 (1993).

[19] G. Bunce, N. Saito, J. Soffer, and W. Vogelsang, Prospects for spin physics at RHIC, Annu. Rev. Nucl. Part. Sci. **50**, 525 (2000).

[20] P. M. Nadolsky and C. P. Yuan, Single spin asymmetries with weak bosons at RHIC, Nucl. Phys. **B666**, 31 (2003).

[21] D. de Florian and W. Vogelsang, Helicity parton distributions from spin asymmetries in W-boson Production at RHIC, Phys. Rev. D **81**, 094020 (2010).

[22] V. Schoefer *et al.*, in Proceedings of IPAC 2012 (unpublished).

[23] K. Adcox *et al.* (PHENIX Collaboration), PHENIX detector overview, Nucl. Instrum. Methods Phys. Res., Sect. A **499**, 469 (2003).

[24] L. Aphecetche *et al.* (PHENIX Collaboration), PHENIX calorimeter, Nucl. Instrum. Methods Phys. Res., Sect. A **499**, 521 (2003).

[25] D. J. C. MacKay, *Information Theory, Inference, and Learning Algorithms* (Cambridge University Press, New York, 2003).

[26] C. E. Rasmussen and K. I. Williams, *Gaussian Processes for Machine Learning* (MIT Press, Boston, 2006).

[27] S. L. Lauritzen, *Graphical Models* (Oxford University Press, New York, 1996).

[28] D. Barber, *Bayesian Reasoning and Machine Learning* (Cambridge University Press, Cambridge, 2012).

[29] T. Sjostrand, S. Mrenna, and P. Z. Skands, PYTHIA 6.4 Physics and Manual, J. High Energy Phys. 05 (2006) 026.

[30] S. S. Adler *et al.* (PHENIX Collaboration), PHENIX on-line and off-line computing, Nucl. Instrum. Methods Phys. Res., Sect. A **499**, 593 (2003).

[31] F. Ringer and W. Vogelsang, Single-spin asymmetries in W boson production at next-to-leading order, Phys. Rev. D **91**, 094033 (2015).

[32] D. de Florian, R. Sassot, M. Stratmann, and W. Vogelsang, Evidence for Polarization of Gluons in the Proton, Phys. Rev. Lett. **113**, 012001 (2014).